The Effect of Bromo Substituents on the Multifaceted Emissive and Crystal Packing Features of Cyclic Triimidazole

Elena Lucenti,[a] Alessandra Forni,*[a] Chiara Botta,*[b] Lucia Carlucci,[c] Alessia Colombo,[c] Clelia Giannini,[c] Daniele Marinotto,[a] Andrea Previtali,[c] Stefania Righetto[c] and Elena Cariati*[c]

[a] Dr. E. Lucenti, Dr. A. Forni
ISTM-CNR, INSTM RU
via Golgi 19, 20133 Milano, Italy.
E-mail: alessandra.forni@istm.cnr.it
[b] Dr. C. Botta
ISMAC-CNR, INSTM RU
Via Corti 12, 20133 Milano, Italy.
E-mail: chiara.botta@ismac.cnr.it
[c] Prof. L. Carlucci, Dr. A. Colombo, Dr. C. Giannini, Dr. D. Marinotto, Dr. A. Previtali, Dr. S. Righetto, Prof. E. Cariati
Dept. of Chemistry, Università degli Studi di Milano and INSTM RU
via Golgi 19, 20133 Milano, Italy.
E-mail: elena.cariati@unimi.it
Supporting information for this article is given via a link at the end of the document.

Abstract: The understanding of the mechanisms involved in crystal packing effects on the photophysical properties of a molecular entity is fundamental to engineer solid materials for specific applications. In fact, besides rigidification and protection from oxygen quenching, crystal packing influences the emissive properties through specific interactions. In the present work, by a critical comparison among the mono- (**1Br**), di- (**2Br**) and tri-bromo (**3Br**) derivatives of triimidazo[1,2-a:1',2'-c:1'',2''-e][1,3,5]triazine, the role of their structural features on the multifaceted emission, spanning from dual fluorescence to ultralong phosphorescence, is elucidated. In particular, conformational distortions are responsible for dual fluorescence, halogen bonding interactions are at the origin of the long lived phosphorescence and π-π interactions resulting into columnar or dimeric H-aggregates induce room temperature ultralong phosphorescence.

Organic materials showing solid state room temperature phosphorescence (RTP) are receiving an ever growing interest because of their many advantages with respect to the organometallic counterparts (e.g. lower toxicity, cost and environmental load).[1] Moreover, specific features associated with organic phosphorescent materials, such as long afterglow lifetimes, have opened the way to new possible applications including low-cost anti-counterfeiting technologies, temperature monitoring, sensing and bio-imaging.[1b]

In solid RTP organic materials, the most evident role of crystal packing is that of suppressing molecular motions so as to minimize the non-radiative deactivation processes of triplet excitons.[2] In addition, densely packed structures can protect from oxygen quenching. However, more specific intermolecular interactions[1c] (e.g. H aggregates,[3] halogen, XB,[4] and hydrogen bonding, HB[5]) can be decisive in activating RTP. The best way to gain insight into the crystal packing effects on the photophysical properties of a molecular entity is, of course, that of analyzing polymorphs, where different packing motifs may give rise to completely different emissive properties.[6] An alternative way to evaluate the crystal packing influence without substantially altering the molecular emissive properties is offered by either regioisomers[7] or compounds containing an increasing number of the same substituent.[2a, 8] Hereafter we report the results of our investigation based on this latter strategy using as substituent Br heavy atoms.

We have recently reported on the intriguing photophysical behaviour of triimidazo[1,2-a:1',2'-c:1'',2''-e][1,3,5]triazine, **TT**,[9] and its mono- and di-bromo derivatives (**1Br** and **2Br**).[8] **TT** is characterized by crystallization induced and mechanochromic emissive behavior, together with room temperature ultralong (1s) phosphorescence (RTUP) at ambient conditions associated with H-aggregation which provides the necessary stabilization of the triplet excitons.[3a] The presence of one or two heavy (Br) atoms on the **TT** scaffold greatly modifies both its molecular and solid state photophysical behaviour. In fact, **1Br** and **2Br** are characterized by a very rich and complex photoluminescence with emissions going from dual fluorescence (2F), molecular phosphorescence (MP) to supramolecular RTP and RTUP.[8] Here we extend our investigation to the tribromo-derivative (namely 3,7,11-tribromotriimidazo[1,2-a:1',2'-c:1'',2''-e][1,3,5]triazine, **3Br**) to get new insight in the relationship between structural and photophysical properties. A critical comparison among **1Br**, **2Br** and **3Br** allows a full understanding of the role of Br atoms on their multifaceted emission and structural features.

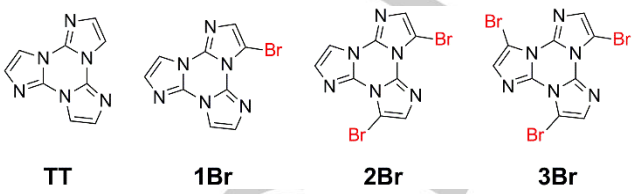

Scheme 1. Chemical structures of the investigated compounds.

Solution

Compounds **1Br**, **2Br** and **3Br** are obtained by bromination of **TT** with N-bromosuccinimide (NBS). **1Br** and **3Br** can be selectively prepared by using 1 (**1Br**, 85% yield) or 3.3 (**3Br**, 90% yield) equivalents of NBS (see Reference 8 and the Supporting Information for experimental details). Addition of 2 equivalents gives a mixture of **1Br** and **2Br** which can be isolated by chromatography.[8]

As previously reported, diluted solutions of **1Br** and **2Br** in CH_2Cl_2 (DCM) display a weak fluorescence by exciting with λ_{exc} over 300nm. At 77K, however, a very intense and broad MP centered at 580nm dominates the spectra by exciting below 280nm (Table 1).

3Br in DCM (10^{-4}M) displays at RT an absorption at about 245nm with an onset at 300nm. Its photophysical behavior resembles that of **1-2Br**, with a hardly discernible emission (370 nm, τ_{av}=10.91ns) at RT and a very broad and intense MP centered at 585nm (τ_{av}=263μs) at 77 K, by exciting below 280 nm (Figure 1, Table 1 and SI).

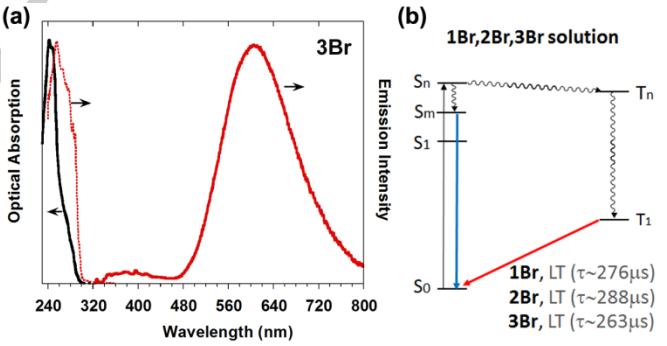

Figure 1. a) Absorption (black line) of **3Br** in DCM (10^{-4}M) at RT. Emission (λ_{exc}=280nm; red solid line) and excitation profile at 77K (λ_{em}=580nm; red dotted line). b) energy level diagram of **1Br**, **2Br** and **3Br** in DCM. Fluorescence and phosphorescence appear as blue and red arrows, respectively.

The TDDFT excitations of **3Br** (Figure S15 and Table S3) are similar to those of **1Br** and **2Br** showing: (i) very weak (for **1Br** and **2Br**) or vanishing (for **3Br**, owing to the symmetry of its π–electronic system) $S_0 \rightarrow S_1$ transition with $^1(\pi,\pi^*)$ character; (ii) subsequent forbidden transition(s) with $^1(\pi,\sigma^*)$ character, where the involved σ orbitals are mainly delocalized on Br atom(s) and C–Br bond(s); (iii) higher energy weak to strong excitations with $^1(\pi,\pi^*)$ character; and (iv) high energy T_n levels with $^3(\sigma,\sigma^*)$ and,

only for **3Br**, $^3(\sigma,\pi^*)$ character. Comparison with the experimental absorption spectra, consisting in two quite close strong peaks followed by one (**1Br** and **2Br**) or two (**3Br**) shoulders at low energy, reveals that the strongest molecular absorption is due to high energy $^1(\pi,\pi^*)$ states, which are also those responsible for the RT emission in solution (denoted with S_m in Table 1). The shoulders observed at lower energies correspond to the weak $^1(\pi,\pi^*)$ excitations to low-lying singlet states. The presence of the $^3(\sigma,\sigma^*)$ and $^3(\sigma,\pi^*)$ T_n levels, which guarantee an efficient intersystem crossing, ISC, (by both El Sayed and heavy atom effects) from the closest S_n levels, fully explains the observed MP (after IC from T_n to T_1) for the three compounds. Such emission, in fact, is only produced by exciting at wavelengths below 280 nm, the energy required to populate the proper S_n levels (Figure 1 right).

Solid State

Single crystal X-ray diffraction studies

Compound **3Br** crystallizes with two independent molecules in the asymmetric unit (Table S2 and Figure S12). The crystal packing of the flat and symmetric (idealized C_{3h} point symmetry) molecules is sustained by different intermolecular interactions *i.e.* Br···Br and Br···N XBs, C-H···N weak HBs, π-π stacking and many van der Waals contacts. Two different orientations of **3Br** molecules are recognizable so that alternating layers of parallel molecules extend in the *ab* directions and perpendicular to *c* (Figure 2 top and S13). Molecules belonging to each layer are involved in columnar π-π interactions characterized by triazinic centroids distances of 4.427, 4.759 and 4.838Å, with the shorter one given by crystallographic different molecules.

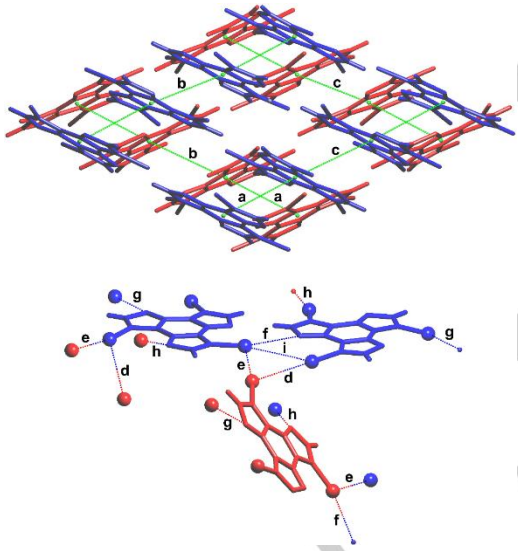

Figure 2. Top: view of the packing along *c* in **3Br**. Two adjacent molecular layers extending parallel to *ab* are shown in red and blue. π-π interactions appear as green lines connecting triazine centroids: 4.4266(4) (**a**), 4.7591(5) (**b**) and 4.8385(5) Å (**c**). Bottom: trimeric unit assembled through Br···Br and Br···N XBs. Br···N interactions **f** and **g**, 3.1344(3) and 3.1545(3) Å respectively, give 1D chains; Br···Br interactions **d** and **e**, 3.5405(3) and 3.6746(3) Å respectively, give layers; Br···N XB **h**, 3.0099(3) Å, extend to 3D; Br···Br contact **i**, 4.1963(14) Å.

A comparison with the π-π stacking in **1Br** and **2Br** evidences that the shortest distance between triazinic centroids in **3Br** (4.427 Å) is significantly shorter than that in **1Br** (4.846 Å) and longer than that in **2Br** (4.068 Å). Moreover, in **1Br** and **2Br** all triazinic centroids are equidistant and aligned parallel to crystallographic directions (*b* for **1Br** and *a* for **2Br**) while in **3Br** they are at three different distances and align the molecules along two different directions ([1,1,0] and [1,-1,0]). To evaluate the presence, if any, of π-π stacking interactions in the three structures, we have computed, within a dimeric unit, the slippage (3.6, 2.3 and 2.9Å for **1Br, 2Br** and **3Br**, respectively) and the angle between the centroid-centroid vector and the projection of this vector on the molecular plane (42, 55 and 48/51° for **1Br**, **2Br** and **3Br** respectively). For **3Br** the values were obtained considering the shortest centroids' distance. Accordingly, strong and reduced slippages are observed for **1Br** and **2Br** respectively, the latter previously described as a H aggregate. In the case of **3Br**, the intermediate slippage is as well indicative of π-π interaction within the selected dimer, so that H dimers, rather than columnar H aggregates, characterize this structure (Figure 3).

Br···Br (**d**, **e**) and Br···N (**h**) XB interactions significantly shorter than the sum of vdW radii involve non-coplanar molecules, except for two short Br···N interactions (**f**, **g**) between coplanar adjacent molecules that give XB chain motifs (Figure 2). The Br···N XB chains run along [1,1,0] and [1,-1,0] directions with a relative inclination of about 50°. Furthermore, adjacent 1D chains are bonded by short Br···Br XBs (**d**, **e**) to give layered motifs that pack along *c* with an *ABAB* sequence. Considering the additional relatively long Br···Br contact (**i**), such layered motif evidences the presence of a trimeric Br_3 XB unit with C–Br···Br angles from 154.8 to 171.5°, in agreement with a type II X···X geometrical arrangement of the X atoms. These layers are further connected by short Br···N interactions (**h**) to give a 3D supramolecular array. Additional Br···Br (3.77-4.20 Å range) and Br···N (3.42-3.57 Å range) interactions longer than the sum of vdW radii are also present. These features are different from what found in **1Br** and **2Br** where Br···N (3.006Å) and Br···Br (3.506 and 3.608Å) interactions, respectively, give dimeric and tetrameric (Br_4) planar units (Figure 3). It is worth to mention that no Br···Br XB are present in **1Br** and that the Br_4 units in **2Br** are involved in Br···N interactions to give layered motifs.

Photophysical studies

As previously reported,[8] powders of **1Br** display at RT dual fluorescence originated by deactivation from both S_1 and a higher S_m level (Table 1 and diagram in Figure 4 top). At 77 K, similar features are observed for excitation above 300nm, while at 280nm the spectrum is dominated by the MP at 573nm already present in solution at 77K. The lacking of UP was justified by the absence of H aggregates. Powders of **2Br** are characterized by a rather complicated emissive behavior associated with the presence of both Br_4 cyclic units and H aggregates in its structure. In fact, at RT a structured fluorescence, a broad long-lived component ($T_1^{Br} \rightarrow S_0$) and a structured RTUP ($T_1^{H} \rightarrow S_0$) are detected. At 77K, a structured fluorescence, very similar to the RT one, appears when exciting at 375nm; a long-lived phosphorescence ($T_1^{Br} \rightarrow S_0$) is observed by exciting at 355nm and the MP at 558nm dominates the spectrum by exciting at 280nm (Table 1 and diagram in Figure 4 bottom).

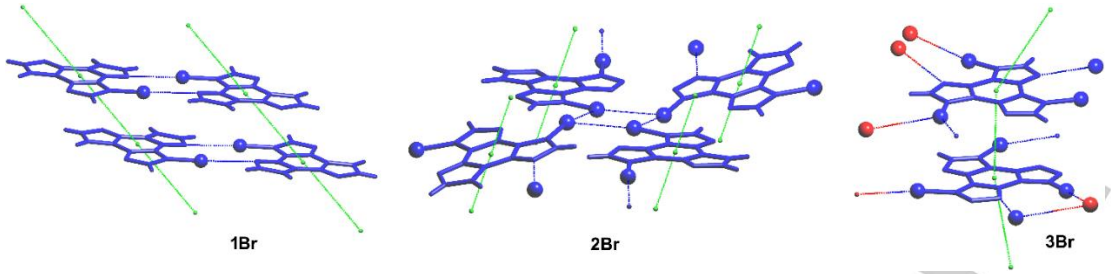

Figure 3. Views of the π-π stacking in **1Br**, **2Br** and **3Br**, Br atoms are shown as spheres and XB interactions are highlighted by blue dashed lines. Red spheres in **3Br** refer to atoms belonging to different layers (see Figure 2 top).

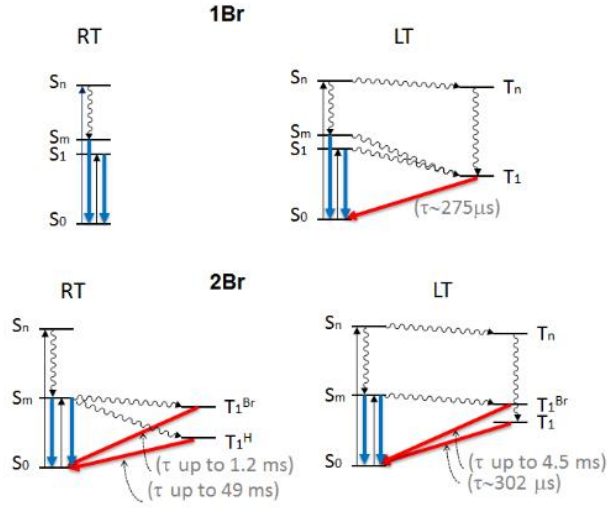

Figure 4. Energy level diagrams showing transitions associated with fluorescence (blue) and phosphorescence (red) respectively for solid **1Br** and **2Br** at 298 (RT) and 77K (LT).

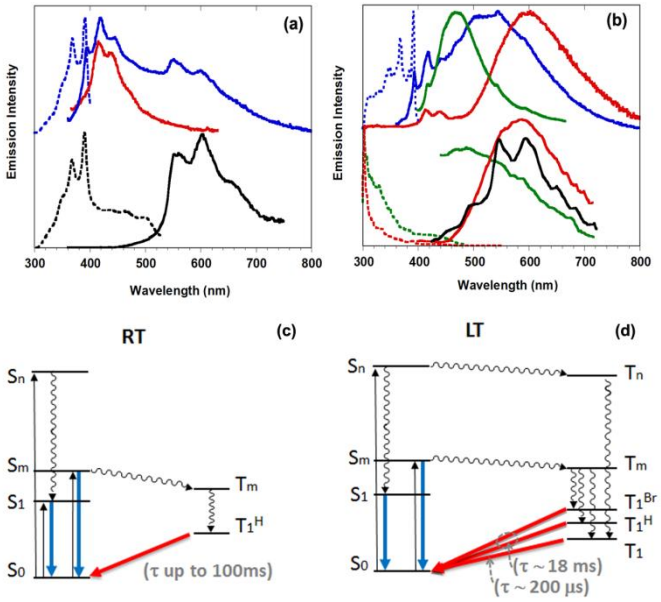

Figure 5. a) Powders of **3Br** at RT. Top: Prompt emission (λ_{exc}=280nm, red solid line; λ_{exc} =340nm, blue solid line) and excitation profile (λ_{em} =420nm, dashed blue line). Bottom: Delayed emission (λ_{exc}=340nm, 1ms delay, window 50 ms; black solid line) and excitation profile (λ_{em}=550nm, dotted black line). b) Powders of **3Br** at 77K. Top: Prompt emission (λ_{exc}=280nm, red solid line; λ_{exc}=340nm, blue solid line; λ_{exc}=385 nm, green solid line) and excitation profile (λ_{em}=420nm, dotted blue line). Bottom: Delayed emission (λ_{exc}=360nm, 100 μs delay, window 500 μs, red solid line; λ_{exc}=385nm, 100 μs delay, window 500 μs, green solid line; λ_{exc}=385nm, 5 ms delay, window 10 ms, black solid line) and excitation profiles (λ_{em}=523nm, dotted green line; λ_{em}=600nm, dotted red line). c) and d) Energy level diagrams showing transitions associated with fluorescence (blue) and phosphorescence (red) at 298 (RT) and 77K (LT) respectively.

Powders of **3Br** at RT (Figure 5a and Table 1) display a structured fluorescence with peaks at 415 and 437nm (τ_{av}=1.02ns, see SI) by exciting at 280nm. With longer wavelength excitation (λ_{exc}=340nm) an additional peak at 394nm is detected together with a lower energy phosphorescence at 555, 605 and 656nm (τ_{av}=18.42ms, see SI). At 77K, the emission becomes even more intricate (Figure 5b and Table 1). Upon excitation at short wavelengths (280 nm) the strong MP at 590 nm (τ_{av}=200μs, see SI), observed in the frozen solutions, dominates the spectrum, while the blue structured fluorescence at 414 and 440nm is still present. By exciting at 340nm the structured fluorescence at 392, 417, 440nm (τ_{av}=1.51ns, see SI) is superimposed to a very broad phosphorescence (τ_{av}=18.11ms, see SI), whose width is reduced by exciting at 385nm. This complex behavior originates from three different phosphorescence contributions better resolved in the delayed spectra (lower panel of Figure 5b). At short delay times (100-600μs) and λ_{exc}=360nm the broad MP is recognizable, while at λ_{exc}=385nm a broad phosphorescence at about 490nm is observed. At longer delay times (>5ms, λ_{exc}=385nm) only the structured phosphorescence, already observed at RT, is present.

To further rationalize the multiple emissive behavior of solid **3Br**, we performed DFT/TDDFT calculations on both dimeric π-π stacked units and trimeric XB Br_3 fragments extracted from the crystal structure and submitted to geometry optimization (due to the non-planarity of the Br_3 unit, it is not possible to extract a reasonably small fragment including at the same time both XB and π-π stacked motifs).

DFT optimization of a π-π dimeric unit of **3Br** resulted in a geometry quite similar to the X-ray one (distances between triazinic centroids equal to 4.254 and 4.4266(4) Å, respectively), associated with strong interaction (-10.12 kcal/mol, corrected for BSSE), close to that obtained for the optimized dimers of **1Br** and **2Br** (-8.43 and -8.53 kcal/mol, respectively). It should however be

noted that, while for **2Br** and **3Br** the distance between centroids remains almost unvaried during optimization, in the case of **1Br** it significantly reduces (to 4.461 Å) with respect to the X-ray value (4.846 Å), accounting for the fact that no UP was observed in the latter case, just owing to weaker π-π interactions in its crystal structure. A collateral observation connected with the different effectiveness of such interactions in the three structures is that the higher energy S_m-S_0 fluorescence of powders of **1Br** is almost unchanged with respect to solution, while for **2Br** and **3Br** it is red-shifted owing to the arising of π-π interactions. Comparison between **2Br** and **3Br** shows that π-π interaction is slightly stronger (by 1.6 kcal/mol) for the latter, though the molecules are further apart from each other (triazinic centroids at 4.254 vs. 4.049 Å in **3Br** and **2Br**, respectively) as observed in the crystal structure.

The 2F, showed by **1Br** and **3Br** in the solid state, should be ascribed to the high energy gap between the strong high energy singlet excitations and the weak S_0-S_1 one. The latter is intensified in solid state owing to the distorting packing forces (Figure S17 and Tables S4, S5). In the case of **3Br** the high energy fluorescence could be described as originated from almost overlapped strong $^1(\pi,\pi^*)$, and weak $^1(\pi,\sigma^*)$ and mixed $^1(\pi,\pi^*)/(\pi,\sigma^*)$ states (the latter two having oscillator strength f=0.01÷0.04), altogether indicated as S_m in Figure 5c and Table 1, falling in a quite restricted (≃0.2 eV) energy range. In the case of **2Br** (Figure S21), fluorescence was previously attributed to deactivation from S_1. Here, a deeper investigation in view of what observed for **3Br**, revealed that a higher S_m is at origin of this emission due to matching of the calculated levels of **2Br** and **3Br**. However, in the case of **2Br** no mixed $^1(\pi,\pi^*)/(\pi,\sigma^*)$ states come out from the computed excitation energies of its π-π dimer, and the $^1(\pi,\sigma^*)$ excitations have f<0.01, suggesting that S_m levels have predominant (π,π^*) character. In the case of **3Br**, the presence of $^3(\pi,\pi^*)$ states (T_m in Figure 5c) very close in energy to $^1(\pi,\sigma^*)$ and mixed $^1(\pi,\pi^*)/(\pi,\sigma^*)$ states (S_m), favor the mixing between singlet and triplet states and may justify the observed phosphorescence of **3Br** from different channels (T_1, T_1^H or T_1^{Br}). In particular, differently from **1Br** and **2Br**, the presence of such manifold states allow to activate the MP exciting even at energy lower than 280nm, a necessary condition for the isolated molecule in solution. On the other side, geometry optimization of the Br_3 unit leads to a coplanar structure with two short (3.702 and 3.751 Å) and one long (3.990 Å) Br···Br distances (Figure S14). The TDDFT computed levels for the Br_3 unit (Figure S19) include a $^3(\pi,\sigma^*)$ state close in energy to a $^1(\pi,\pi^*)$ one suggesting that efficient spin-orbit coupling may occur between the two states allowing T_1^{Br} phosphorescence. Interestingly, such triplet is the only one involving excitations towards σ* orbitals mainly delocalized on the three XB Br atoms (MOs 335 and 338 in Figure S20), supporting the role of the Br_3 unit in the intermolecular electronic coupling[10] responsible for the phosphorescence. However, the planarity of the optimized fragment suggests reduced stability associated with the Br_3 XB motif in the crystal of **3Br**, differently from the planar Br_4 motif found in the crystal of **2Br**. This could account for the missing observation of phosphorescence from T_1^{Br} in **3Br** at RT with respect to **2Br** and the fact that UP due to H-aggregation is observed for **3Br** also at LT, while in **2Br** it is overwhelmed by emission from T_1^{Br}.

In conclusion, by combined structural, photophysical and theoretical results we give further insights into the mechanisms involved in the crystal packing/emission relationship of organic compounds. Besides rigidification and protection from oxygen quenching, the crystal packing can in fact influence the emissive properties through: i) conformational distortions, ii) specific intermolecular interactions and iii) supramolecular effects. This is clearly demonstrated by a comparison among **3Br** and the previously reported **1Br** and **2Br**, whose behavior is here critically reviewed and whose hidden aspects (i.e. fluorescence from a S_m rather than S_1 level) discovered thanks to the results obtained for the added member of the family. These compounds display the same emissive properties in solution, in agreement with only slightly modified electronic properties, but quite different ones in the solid state. The comparison among the three derivatives has allowed to disclose the following effects of crystal packing: i) conformational distortions are responsible for the appearance of the S_1-S_0 emission in **1Br** and **3Br**; ii) intermolecular interactions manifest in a different way according to their strength; in particular the stronger and more rigid Br_4 XB unit of **2Br** is responsible for a long lived RTP which is absent in **3Br** having a looser not planar Br_3 XB unit; iii) π-π interactions result into columnar or dimeric aggregates characterized by slippage increasing in the order **2Br**<**3Br**<**1Br**; the reduced slippage in **2Br** and **3Br**, described as H-aggregates, explains their RTUP.

It is the relative strength of these interactions which determines the RT luminescent behavior. A comprehensive understanding of the molecular and intermolecular mechanisms provides fundamentals tools for engineering materials in view of specific applications.

Table 1. Photoluminescence data at 298 and 77K. Values for **1Br** and **2Br** are taken from reference 8.

Sample	298 K			77 K		
	λ_{em} (nm)	τ_{av}[a]	origin	λ_{em} (nm)	τ_{av}[a]	origin
1Br (DCM)	328, 342, 358[b]	0.68 ns	S_m-S_0	580[c]	276 µs	T_1-S_0
1Br (pwd)	326, 345, 365, 382[b]	0.89 ns	S_m-S_0	344, 365, 378 (sh)[d]	0.86 ns	S_m-S_0
	426, 530[e]	5.52 ns	S_1-S_0	457, 492, 530[d]	2.54 ns	S_1-S_0
				573[c]	274 µs	T_1-S_0
2Br (DCM)	380[b]	5.21 ns	S_m-S_0	575[c]	288 µs	T_1-S_0
2Br (pwd)	395, 419, 443[b]	0.91 ns	S_m-S_0	409, 434, 462[f]	1.96 ns	S_m-S_0
	470[g]	1.07 ms	T_1^{Br}-S_0	433 (sh), 461, 484[e]	4.05 ms	T_1^{Br}-S_0
	553, 600, 646[h]	28.85 ms	T_1^{H}-S_0	558[c]	302 µs	T_1-S_0
3Br (DCM)	370[b]	10.91 ns	S_m-S_0	585[c]	263 µs	T_1-S_0
3Br (pwd)	394, 418, 444[i]	1.02 ns[j]	S_m-S_0	392, 417, 440 (sh)[i]	1.51 ns[j]	S_m-S_0
	415, 437 (sh)[c]		S_1-S_0	414, 440[c]		S_1-S_0
				490[k]		T_1^{Br}-S_0
	555, 605, 656 (sh)[i]	18.42 ms	T_1^{H}-S_0	545, 596, 650[k]	18.11 ms	T_1^{H}-S_0
				590[c]	200 µs	T_1-S_0

[a] $\tau_{av} = \sum \frac{A_i t_i^2}{A_i t_i}$.; [b] λ_{exc} = 300 nm; [c] λ_{exc} = 280 nm; [d] λ_{exc} = 310 nm; [e] λ_{exc} = 350 nm; [f] λ_{exc} = 375 nm; [g] λ_{exc} = 370 nm; [h] λ_{exc} = 360 nm; [i] λ_{exc} = 340 nm; [j] λ_{exc} = 300 nm, λ_{em} = 433 nm; [k] λ_{exc} = 385 nm.

Acknowledgements

The use of instrumentation purchased through the Regione Lombardia−Fondazione Cariplo joint SmartMatLab Project is gratefully acknowledged.

Keywords: H aggregates• halogen bonding • photophysics • room temperature phosphorescence • time resolved spectroscopy

[1] a) M. Baroncini, G. Bergamini, P. Ceroni, *Chem. Commun.* **2017**, *53*, 2081-2093; b) S. Hirata, *Adv. Opt. Mater.* **2017**, *5*, 1700116; c) A. Forni, E. Lucenti, C. Botta, E. Cariati, *J. Mater. Chem. C* **2018**, *6*, 4603-4626.

[2] a) Y. Gong, G. Chen, Q. Peng, W. Z. Yuan, Y. Xie, S. Li, Y. Zhang, B. Z. Tang, *Adv. Mater.* **2015**, *27*, 6195-6201; b) W. Z. Yuan, X. Y. Shen, H. Zhao, J. W. Y. Lam, L. Tang, P. Lu, C. Wang, Y. Liu, Z. Wang, Q. Zheng, J. Z. Sun, Y. Ma, B. Z. Tang, *J. Phys. Chem. C* **2010**, *114*, 6090-6099; c) Z. He, C. Ke, B. Z. Tang, *ACS Omega* **2018**, *3*, 3267-3277.

[3] a) Z. An, C. Zheng, Y. Tao, R. Chen, H. Shi, T. Chen, Z. Wang, H. Li, R. Deng, X. Liu, W. Huang, *Nat. Mater.* **2015**, *14*, 685-690; b) M. Kasha, H. R. Rawls, M. Ashraf El-Bayoumi, *Pure Appl. Chem.* **1965**, *11*, 371-392.

[4] a) H. Shi, Z. An, P.-Z. Li, J. Yin, G. Xing, T. He, H. Chen, J. Wang, H. Sun, W. Huang, Y. Zhao, *Cryst. Growth Des.* **2016**, *16*, 808-813; b) O. Bolton, K. Lee, H.-J. Kim, K. Y. Lin, J. Kim, *Nat. Chem.* **2011**, *3*, 205-210.

[5] S. Cai, H. Shi, Z. Zhang, X. Wang, H. Ma, N. Gan, Q. Wu, Z. Cheng, K. Ling, M. Gu, C. Ma, L. Gu, Z. An, W. Huang, *Angew. Chem. Int. Ed.* **2018**, *57*, 4005-4009.

[6] a) C. Botta, S. Benedini, L. Carlucci, A. Forni, D. Marinotto, A. Nitti, D. Pasini, S. Righetto, E. Cariati, *J. Mater. Chem. C* **2016**, *4*, 2979-2989; b) J. Yang, Z. Ren, B. Chen, M. Fang, Z. Zhao, B. Z. Tang, Q. Peng, Z. Li, *J. Mater. Chem. C* **2017**, *5*, 9242-9246.

[7] a) Y. Liu, G. Zhan, P. Fang, Z. Liu, Z. Bian, C. Huang, *J. Mater. Chem. C* **2017**, *5*, 12547-12552; b) S. Cai, H. Shi, D. Tian, H. Ma, Z. Cheng, Q. Wu, M. Gu, L. Huang, Z. An, Q. Peng, W. Huang, *Adv. Funct. Mater.* **2018**, 1705045.

[8] E. Lucenti, A. Forni, C. Botta, L. Carlucci, C. Giannini, D. Marinotto, A. Pavanello, A. Previtali, S. Righetto, E. Cariati, *Angew. Chem. Int. Ed.* **2017**, *56*, 16302-16307.

[9] E. Lucenti, A. Forni, C. Botta, L. Carlucci, C. Giannini, D. Marinotto, A. Previtali, S. Righetto, E. Cariati, *J. Phys. Chem. Lett.* **2017**, *8*, 1894-1898.

[10] Z. Yang, Z. Mao, X. Zhang, D. Ou, Y. Mu, Y. Zhang, C. Zhao, S. Liu, Z. Chi, J. Xu, Y.-C. Wu, P.-Y. Lu, A. Lien, M. R. Bryce, *Angew. Chem. Int. Ed.* **2016**, *55*, 2181-2185.

Entry for the Table of Contents

COMMUNICATION

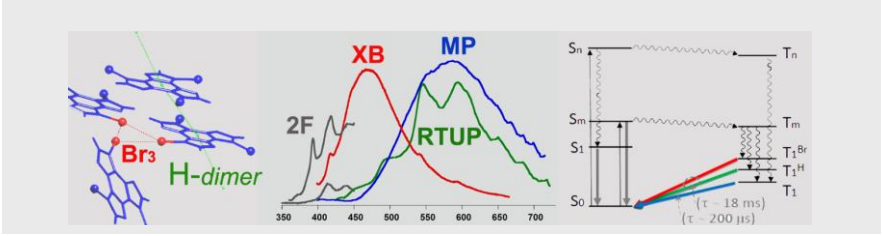

Besides rigidification and protection from oxygen quenching, crystal packing influences the emissive properties through specific interactions which, in mono-, di- and tri-bromo derivatives of cyclic triimidazole, are responsible for multifaceted emission. Conformational distortions are associated to dual fluorescence, halogen bonding interactions are at the origin of long lived phosphorescence and columnar or dimeric H-aggregates induce room temperature ultralong phosphorescence.

Elena Lucenti, Alessandra Forni, Chiara Botta,* Lucia Carlucci, Alessia Colombo, Clelia Giannini, Daniele Marinotto, Andrea Previtali, Stefania Righetto and Elena Cariati**

Page No. – Page No.

The Effect of Bromo Substituents on the Multifaceted Emissive and Crystal Packing Features of Cyclic Triimidazole